Materials Research. 2017; 20(3): 853-859
DOI: http://dx.doi.org/10.1590/1980-5373-MR-2016-0627

The Analysis of the Microstructure and Mechanical Properties of Low Carbon Microalloyed Steels after Ultra Fast Cooling

Yong Tian[a], Hong-tao Wang[a], Yong Li[a]*, Zhao-dong Wang[a], Guo-dong Wang[a]

[a] *State Key Laboratory of Rolling and Automation, Northeastern University, Shenyang, China*

Received: August 31, 2016; Revised: March 10, 2017; Accepted: April 9, 2017

In this paper, two low carbon microalloyed steels, named as steel A and steel B, were fabricated by ultra fast cooling (UFC). In both steels, the microstructures containing quasi polygonal ferrite (QF), acicular ferrite (AF) and granular bainite (GB) can be obtained by UFC process. The amount of AF in steel B is more than that in steel A. The size and distribution of precipitates (Nb/Ti carbonitrides) in steel B are finer and more dispersed than those of in steel A due to relatively low finish cooling temperature. The mechanical properties of both steels are effectively enhanced by UFC process. UFC process produces low-temperature transformation microstructures containing a significant amount of AF. The mechanical properties of steel B were more satisfactory than those of steel A due to the finer average grain size, the greater amount of the volume fractions and smaller size of secondary phases.

Keywords: *Low carbon microalloyed steels, Ultra fast cooling (UFC), Acicular ferrite (AF), The mechanical properties*

1. Introduction

High-strength low-alloy (HSLA) steels are those high-strength structural steels having good toughness and weldability. This combination of properties have led to their varied applications in the automotive industry, in manufacturing of large diameter pipes for gas and oil transportation in the areas of low temperature, and in fabrication of plates for naval ship's construction[1]. It is also popular to use HSLA steels replacing the conventional low strength counterpart for reducing thicknesses and permitting the reduction of weight in weight-saving applications[2]. The wide range of mechanical properties attainable in HSLA steels coupled with their relatively low cost are responsible for their high volume of production, which represents ~10% of the world's steel production[3]. The evolution of HSLA steel was based on low carbon content to improve weldability and suitable alloying elements were added to improve austenite hardenability[4-6]. Thermomechanical controlled processing (TMCP) and microalloying in order to obtain desired microstructure and properties are the essence of ultra-low carbon microalloyed steel[7]. TMCP has become the most powerful and effective manufacturing process to satisfy increased hardenability, improved strength, and superior low-temperature toughness[8]. The microstructure, which is related with the mechanical properties of the hot rolled steels, is heavily influenced by the cooling process after hot rolling. The ultra fast cooling (UFC) technology was applied in order to get faster cooling rate. The cooling rate of UFC is more than twice that of traditional ACC (20ºC/s for 20mm)[9]. UFC process enhances strengthening associated with precipitation and grain refinement[10]. The microstructure and mechanical properties of low carbon microalloyed steel can be significantly improved by UFC process after hot deformation[11].

This article presents an analysis of the final microstructure of two low carbon microalloyed steels after UFC process. Tensile and Charpy impact tests at room temperature and lower temperature were performed, respectively, to evaluate strength and toughness. The key objective of this study was to discuss and determine the strengthening contribution of the morphologies of ferrite, bainite and the detected Nb/Ti (C, N) carbonitrides in the two experimental steels subjected to UFC process.

2. Experimental Procedure

Two types of low-alloyed, low-carbon steels were produced in terms of different content of Cr, Mo and Ni. Plates with thickness of 250 mm were used for rolling mill tests. The cylindrical rod specimens with 8 mm diameter and 15 mm length were machined from the plates in order to measure the transformation temperature in a thermomechanical simulator. The austenite nonrecrystallization temperature (T_{nr}) was evaluated through softening fraction-interpass time curves. It was calculated by the back extrapolation method[12]. The Ar_3 and Ar_1, which denote the start and finish temperatures of the austenite-to-ferrite transformation, respectively, were measured using the thermomechanical simulator. A schematic illustration of the double-pass compression test to measure Ar_3 and Ar_1 is shown in Figure 1. In Figure 1, specimens were heated at a rate of 50ºC/s, solution treated at 1150ºC for 180 s, deformed to 30% compressive strain at

* e-mail: neu81@126.com

$1s^{-1}$, cooled to 920ºC at 5ºC/s, deformed to 40% compressive strain at $1s^{-1}$. Then, the specimens were cooled at 30ºC/s to room temperature. The chemical compositions and measured transformation temperature (T_{nr}, Ar_3 and Ar_1) of the steels are listed in Table 1.

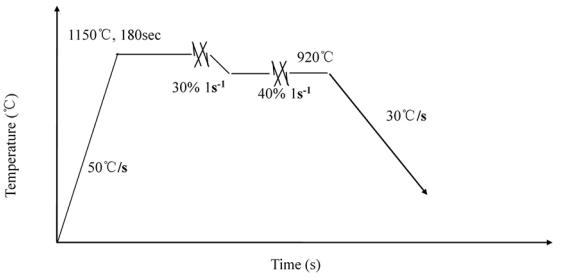

Figure 1. Schematic illustration of measuring Ar_3 and Ar_1.

After being hold for 280 min at a soaking temperature of 1200ºC, the rough-rolling temperature started at 1150ºC above the nonrecrystallization temperature of austenite for both steels. The finish-rolling stage was started at 920ºC and finished rolling at 820ºC. The rolled plates were air-cooled to the start cooling temperature of 780ºC, were water-cooled to 550ºC and 460ºC at a cooling rate of 30ºC/**s**, and then were air-cooled for steel A and B, respectively. The processing schedule of the experimental steels is shown in Figure 2. As a result, the final plates with thickness of 17.5 mm and 19.3 mm for steel A and B, respectively, were obtained.

Five tensile and Charpy impact specimens were collected from various positions along the center-line of the plates, respectively. The flat tensile specimens, 160 mm in total length, 20 mm in effective width, 17.5/19.3 mm in thickness and 50 mm in gauge length, were machined from the plates with the longitudinal axis parallel to the longitudinal direction, and tensile tests were carried out on an INSTRON 4206 machine at a strain rate of 5 mm min^{-1}. The Charpy impact specimens direction were also paralleled to the rolling direction. The tensile specimens were tested at room temperature, and impact tests of steels A and B were performed at -10ºC and -15ºC, respectively, according to Chinese standard to obtain an averaged result[13]. The Vickers hardness tester was used to measure the Vickers hardness with 10-kg load. The microstructures of the transverse section of the specimens were examined with an optical microscopy (OM) after a LePera etching[14] and with a scanning electron microscopy (SEM) after conventional 4% Nital etching. Thin specimens were observed in a transmission electron microscopy (TEM) with energy dispersive spectrometry (EDS) facility. Volume fractions of phases present in the plates were measured by an image analyzer.

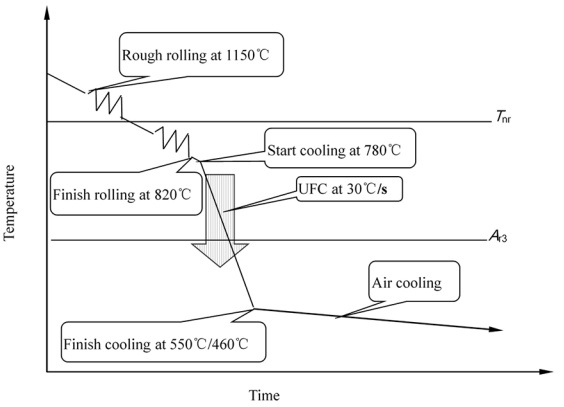

Figure 2. The processing schedule of the experimental steels.

3. Experimental Results

3.1. Tensile and charpy impact properties

Yield strength ($R_{t0.5}$), ultimate tensile strength (R_m), yield ratio ($R_{t0.5}/R_m$), total elongation (A_{50}), the Charpy absorbed energy (A_K) and Vickers hardness (HV10) of the specimens after UFC process are summarized in Table 2. Apparently, steel B has higher values than steel A. The Charpy absorbed energies of steel A at -10ºC are higher than 436J, and those of steel B at -15ºC are higher than 396J. The hardness values of steel B are also higher than those of steel A.

Average ultimate tensile and yield strength, yield ratio, total elongation and the Charpy absorbed energy of both steels are shown in Figure 3. In Figure 3, steel B has higher average value of strengths than that of steel A. Furthermore, the Charpy absorbed energies level of steel B at -15ºC is only slightly lower than those of steel A at -10ºC, despite microalloying and UFC process result in higher strength and higher hardness for the former.

3.2. Microstructures

OM and SEM micrographs of both steels are shown in Figure 4 and Figure 5. In Figure 4, ferrite appears gray, bainite appears dark, and both martensite and retained austenite appear white since they are difficult to be tinted in LePera etchant[14]. By visual inspection, all specimens are mostly composed of quasi polygonal ferrite (QF), acicular ferrite (AF) and granular bainite (GB). The GB contains equiaxed,

Table 1. Chemical composition (wt %) and measured transformation temperature (ºC) of both steels.

Steel	C	Si	Mn	P	S	Nb	Cr	Ni	Cu	Mo	Ti	B	T_{nr}	Ar_3	Ar_1
A	0.086	0.170	1.590	0.012	0.005	0.074	0.020	0.010	0.020	0.002	0.013	0.0003	950	590	480
B	0.054	0.220	1.710	0.004	0.001	0.072	0.241	0.202	0.012	0.129	0.012	0.0002	975	600	490

Table 2. Mechanical properties of the experimental steels.

Specimen No.		R_t0.5/MPa	R_m/MPa	R_t0.5/ R_m	A_{50}/%	A_K/J	HV10
Steel A	A-1	555	615	0.9	41	436 at -10ºC	219
	A-2	530	615	0.86	40	408 at -10ºC	218
	A-3	535	600	0.89	44	288 at -10ºC	207
	A-4	515	600	0.86	40	345 at -10ºC	205
	A-5	530	620	0.85	41	385 at -10ºC	220
Steel B	B-1	590	675	0.87	35	394 at -15ºC	232
	B-2	530	685	0.77	32	371 at -15ºC	249
	B-3	535	680	0.79	34	361 at -15ºC	238
	B-4	570	680	0.84	37	396 at -15ºC	243
	B-5	540	680	0.79	38	331 at -15ºC	242

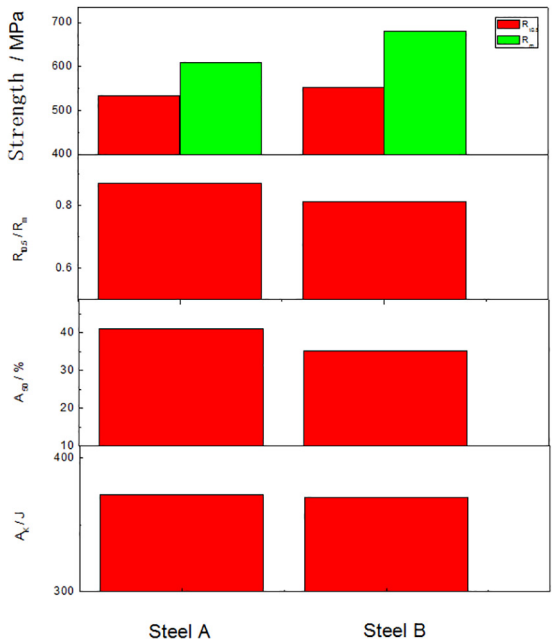

Figure 3. Average properties of both steels.

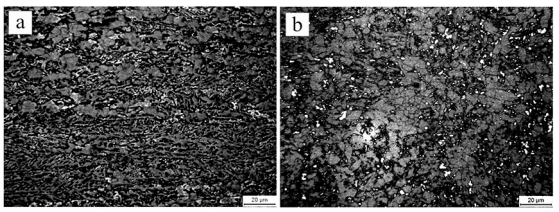

(a) Specimen A-5 (b) Specimen B-2

Figure 4. Optical micrographs of specimens after UFC process.

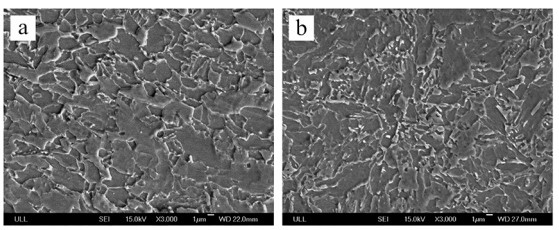

(a) Specimen A-5 (b) Specimen B-2

Figure 5. SEM micrographs of specimens after UFC process.

island-shaped martensite-austenite (MA) constituents. QF and AF ferrite coexist in the microstructure. The QF grains have irregular and jagged boundaries, containing subboundaries. The AF is an acicular microstructure formed inside austenite grains and contains MA at irregularly shaped grain boundaries. Steel A is mostly composed of QF together with a very small amount of pearlite (P). Steel B mostly consists of AF, together with GB, instead of P.

The volume fractions of secondary phases were evaluated and the results are shown in Table 3. Secondary phases are mainly retained austenite and martensite-austenite constituents, and cementite can be ignored for low carbon content (0.086% maximum). The volume fraction of MA tends to be higher in steel B than that in steel A. A large number of M-A islands in steel B are fine and dispersed (Figure 5, Table 3).

SEM micrographs of the fracture surface of the Charpy impact specimens fractured at -10ºC for specimen A-5 and at -15ºC for specimen B-2, are shown in Figure 6. In Figure 6, a lot of dimples were found. The fracture appearance of steel B still exhibits toughness characteristics even the fracture occurs at low temperature.

The TEM of specimens reveals the presence of quasi polygonal ferrite (QF) and acicular ferrite (AF), martensite-austenite (MA) island, dislocation and carbide precipitation at the bainitic ferrite platelet (Figures 7, 8, 9, 10 and 11). Specimen A-5 exhibits a mixture of QF and AF microstructure as shown in Figure7 (a). Large amounts of AFs are found in specimen B-2 as shown in Figure7 (b). The presence of islands of MA component within QF and/or AF structure is further confirmed by the TEM studies (Fig. 8). In Figure8 (b), fine AFs are largely observed, while MA is homogeneously dispersed. A fairly high dislocation density in QF and/or AF is an essential characteristic of transformation product (Fig. 9). The precipitates with diameters in the ranges 8-40 nm and 5-30 nm for steel A and B were observed by TEM which were shown in Figure 10 (a) and 11 (a). The EDS image shown in Figure 10 (b) and 11 (b) taken from the precipitate particle

Table 3. Average grain size and the size and the volume fractions of secondary phases.

Steel	Quasi polygonal ferrite	Acicular ferrite	Granular bainite/%	Average grain size/μm	The volume fractions of secondary phases/%	The size of secondary phases/μm	Average size of secondary phases/μm
A	Bal.	-	-	10.34 ± 2.3	12.67 ± 0.4	4.32~5.94	5.18 ± 0.1
B	-	Bal.	-	9.47 ± 2.6	17.73 ± 0.5	3.54~5.12	4.36 ± 0.3

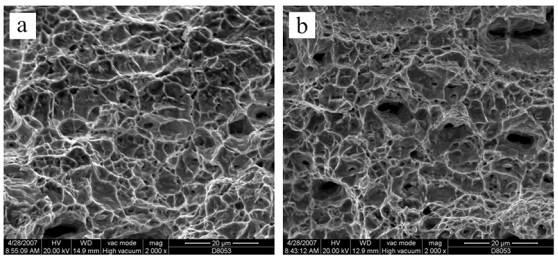

(a) Specimen A-5 (b) Specimen B-2

Figure 6. Fractographs of Charpy impact specimens fractured at -10ºC and -15ºC.

reveals that the particle is enriched with Nb, Ti, C and N. The results denote the presence of carbonitrides precipitates of niobium and titanium, Nb/Ti (C, N).

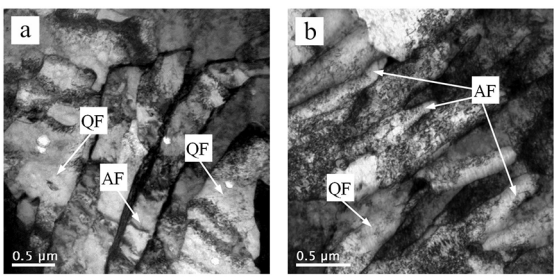

(a) Specimen A-5 (b) Specimen B-2

Figure 7. TEM micrographs of specimens showing the formation of quasi polygonal ferrite (QF) and acicular ferrite (AF).

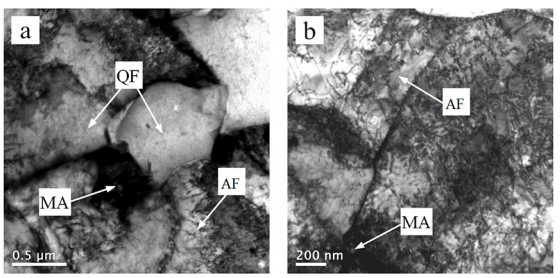

(a) Specimen A-5 (b) Specimen B-2

Figure 8. TEM micrographs of specimens showing the presence of MA island.

4. Discussion

Two low-carbon steel alloyed with Si, Mn, Cr and Mo and microalloyed with Nb, Ti and Ni have been designed. The low carbon is preferred for the current steel from the viewpoint of low segregation, good toughness, and superior

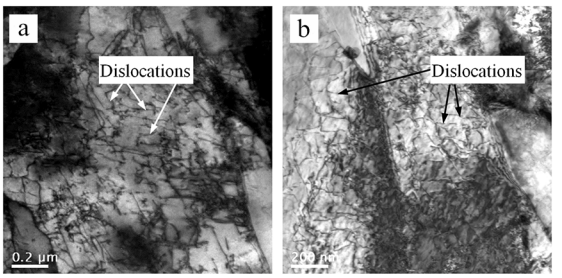

(a) Specimen A-5 (b) Specimen B-2

Figure 9. TEM micrographs of dislocations in ferrite observed in specimens.

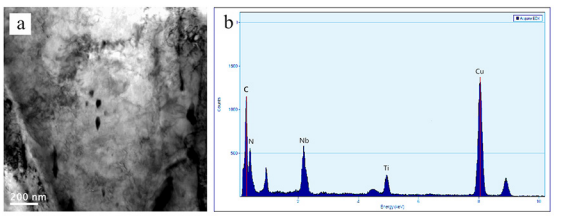

(a) the precipitate particles (b) EDS image

Figure 10. TEM micrograph of specimen A-5 showing the presence of carbonitrides precipitates.

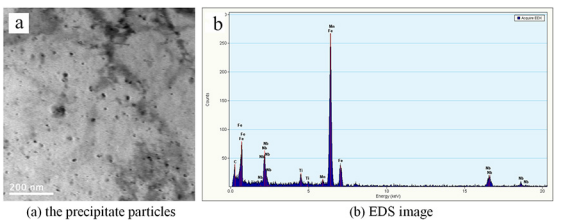

(a) the precipitate particles (b) EDS image

Figure 11. TEM micrograph of specimen B-2 showing the presence of carbonitrides precipitates.

weldability. The addition of Si, Mn, Cr, Mo and other alloying elements increase the hardenability of austenite. Austenite has been stabilized up to a very low temperature, and γ→α transformation has been retarded. Cr, Mo and Ni have been added at a balanced level in steel B, which improves austenite hardenability. Mo retards separation of ferrite from parent austenite and depresses Bs temperature. The amount of GB in steel B is higher than that in steel A (Fig. 5). This is attributed to the presence of Mo in steel B.

The soaking temperature (1200ºC) and time (280 min) adopted in the current study essentially control the composition and grain size of austenite. The high soaking temperature and time are employed to ensure the maximum dissolution of microalloying carbides and carbonitrides in austenite. At

this high soaking temperature, austenite grain growth would be restricted by fine Nb/Ti (C, N) particles. A controlled precipitation process of carbides, nitrides and carbo-nitrides formed during the TMCP is responsible for the fine-grained ferritic structure. The finish-rolling temperature is lower than the nonrecrystallization temperature (Table 1) of austenite present in the steel and therefore static recrystallization of austenite is ruled out. The pancaked grains are formed due to rolling in the nonrecrystallized austenite region. Dynamic recrystallization is likely to occur as strain accumulation takes place from one roll pass to another in the absence of static recrystallization[4]. The rolling at γ nonrecrystallization region accumulates a strain (i.e., dislocations) in austenite grains and this strain can promote the ferrite grain refinement by acting as a nucleation site for γ-α transformation[15]. The average ferrite grain size relates to thickness of pancaked austenite grain, alloying elements that depress austenite to ferrite transformation and ultra fast cooling (UFC) from austenite region. The grain refinement effect is sufficiently achieved by the controlled rolling process at high temperatures, and low-temperature transformation microstructures are formed by the accelerated cooling process[16]. UFC process is favorable to the formation of ferrite nuclei and results in the fine ferrite grains (Fig. 4, 5 and Table 3).

In general, with increased cooling rate the nature and morphology of ferrite alters from polygonal to plate-type or elongated and subsequently to lath and acicular type ferrite[17]. UFC process promotes the formation of acicular ferrite (Fig. 7). According to Lu et al.[18], a combination of high cooling rate and low coiling temperature/interrupted cooling temperature in microalloyed steels helps to produce a fine bainitic/acicular ferrite microstructure, making higher strength steels possible. It is worth noting that it is easy for a rolling mill to produce steel products under relative higher temperature rolling because the load is not heavy during rolling. Therefore, the enhancement of the finishing rolling temperature (820ºC) of the present steel is favorable for practice mill. On the other hand, a considerable amount of AFs in the high start cooling temperature (780ºC) condition is formed. It has been well accepted that the AF, in the GB microstructure, comes from a mixed diffusion and shear transformation mode during continuous cooling beginning at a temperature above the upper bainite transformation region temperature[19]. The AF nucleates at intragranular sites and it is characterized by an assemblage of interwoven non-parallel ferrite laths with high density of tangled dislocations, where the most parts of the neighboring lath (subgrain) boundaries have dissimilar orientations[19]. A microstructure of acicular ferrite has the potential of combining high strength and high toughness, because a crack would have to follow a more tortuous path through a microstructure of acicular ferrite[20]. As mentioned above, the structure of steel A presents a smaller amount of acicular ferrite than steel B. The enhanced mechanical properties are related to that the microstructures are composed mainly of low-temperature transformation microstructures (AF) in steel B (Table 2, Fig. 3).

It was already mentioned that GB is an equiaxed microstructure, and contains island-type MA constituents. It is well known that MA is mainly generated at rapid cooling rates and low finish cooling temperatures[16]. The volumetric fraction of M-A islands increases because of higher cooling rates[20]. The size of MA tended to decrease with increasing finish cooling temperature. As hard secondary phases such as MA are readily transformed at low temperatures[21], therefore, both steels show high strength due to UFC process, except for the action of Mo in the steel[22]. This is also the reason for that the strengths of steel B were higher than those of steel A because of the strengthening contribution due to the MA constituent (Fig. 8).

As mentioned previously, QF and/or AF contain a high dislocation density (Fig. 9). This is because UFC process would help to keep more dislocations introduced by deformation. The strength is mainly decided by the barriers to movement of dislocation line and deviate from M-A islands[10]. Therefore, high strength levels were obtained for both steels, and steel B ontaining a higher volume fraction and greater dispersion of MA showed higher yield and tensile strengths.

The fine particle precipitation directly comes from UFC process after hot deformation for both steels. When several of the microalloyed elements are present in the alloy, the precipitated carbides or carbonitrides have a complex composition of Ti, Nb and V being more effective as strengthener in the steel[19,22]. The suppression of grain boundary migration due to microalloying is caused by either the solute dragging effect caused by segregation of alloying elements to the boundaries, or the pinning effect caused by carbo-nitride precipitates. These very fine precipitates are responsible for the fine-grained ferritic structure[23]. Noting that the size and distribution of precipitates (Nb/Ti carbonitrides) in steel B are finer and more dispersed than those of in steel A (Fig. 10, 11). Despite the precipitates reduced the absorbed energy by facilitating a ductile fracture, the fine precipitation of the different carbides or carbonitrides (TiCN, NbCN) during the hot-rolling provides an additional precipitation strengthening in the final steel plate.

There is some solid solution strengthening from the addition of alloying elements in two low carbon steels. UFC process also results in the dislocation strengthening. Moreover, the improvement of mechanical properties also results mainly from the refinement of ferrite grain size and precipitation strengthening. When the cooling rate increases, the grain size decreases overall, and the volume fraction of bainitic ferrite increases, which leads to the higher strength and the lower ductility and toughness[16]. The fine particle precipitation contributes to the strengthening of the steel[19]. However, the Charpy absorbed energies of steel B do not significantly reduce (Table 2 and Fig. 3). It is well known that the addition of Ni significantly increases the toughness

and lowers the ductile brittle transition temperature in the steels. On the other hand, Charpy impact absorbed energy is proportional to the volume fraction of acicular ferrite[16]. Microstructures with a significant proportion of acicular ferrite (AF) have an optimized combination of mechanical properties in both steels after UFC process. This is in rather good agreement to the other authors' findings[20]. As mentioned above, the size of secondary phases decreases with decreasing finish rolling temperature (Fig. 5, Table 3). The yield strength is reduced when the finish cooling temperature decreases further below a certain temperature, as suggested by Sung[16]. As a result, steel B exhibits high strengths, as well as relatively low yield ratio. Satisfactory mechanical properties can be obtained by UFC process for two low carbon microalloyed steels.

5. Conclusions

(1) The microstructures containing QF, AF and GB in low carbon microalloyed steels can be obtained mainly by UFC process. The amount of AF in steel B is more than that in steel A. The size and distribution of precipitates (Nb/Ti carbonitrides) in steel B are finer and more dispersed than those of in steel A due to relatively low finish cooling temperature.

(2) The mechanical properties of both steels are effectively enhanced by UFC process. This is attributed to the strengthening contribution caused by solid solution, grain refinement, dispersion, dislocation and precipitation strengthening. The mechanical properties of steel B are more satisfactory than those of steel A due to the finer average grain size, the greater amount of the volume fractions and the smaller size of secondary phases.

(3) UFC process produces low-temperature transformation microstructures containing a significant amount of AFs. Crack propagation would have to follow a more tortuous path through a microstructure of acicular ferrite. Therefore, an optimized combination of mechanical properties can be obtained in both steels. This is also a reason for that the mechanical properties of steel B were higher than those of steel A.

6. Acknowledgment

This work was subsidized by the Natural Science Foundation of China (Grant No.51234002) and the national key research and development program(Grant No. 2016YFB0300701 & 2016YFB0300605). The authors are also grateful to the staff of Qinhuangdao Shouqin Metal Materials Co, Ltd.

7. References

1. Khaki DM, Ayaz M, Arab NBM, Noroozi A. Multiresponse Optimization of Mechanical Properties and Formability of Hot Rolled Microalloyed Steels. *Journal of Materials Engineering and Performance*. 2013;23(3):1002-1015.

2. Misra RDK, Nathani H, Hartmann JE, Siciliano F. Microstructural evolution in a new 770 MPa hot rolled Nb-Ti microalloyed steel. *Materials Science and Engineering: A*. 2005;394(1-2):339-352.

3. Pereloma EV, Kostryzhev AG, AlShahrani A, Zhu C, Cairney JM, Killmore CR, et al. Effect of austenite deformation temperature on Nb clustering and precipitation in microalloyed steel. *Scripta Materialia*. 2014;75:74-77.

4. Shukla R, Das RK, Ravi Kumar B, Ghosh SK, Kundu S, Chatterjee S. An Ultra-low Carbon, Thermomechanically Controlled Processed Microalloyed Steel: Microstructure and Mechanical Properties. *Metallurgical and Materials Transactions A*. 2012;43(12):4835-4845.

5. Kim J, Jung JG, Kim DH, Lee YK. The kinetics of Nb(C,N) precipitation during the isothermal austenite to ferrite transformation in a low-carbon Nb-microalloyed steel. *Acta Materialia*. 2013;61(19):7437-7443.

6. Khalaj G, Nazari A, Livary AK. Application of ANFIS for modeling of microhardness of high strength low alloy (HSLA) steels in continuous cooling. *Materials Research*. 2013;16(4):721-730.

7. Xie H, Du LX, Hu J, Misra RDK. Microstructure and mechanical properties of a novel 1000 MPa grade TMCP low carbon microalloyed steel with combination of high strength and excellent toughness. *Materials Science and Engineering: A*. 2014;612:123-130.

8. Bandyopadhyay PS, Ghosh SK, Kundu S, Chatterjee S. Evolution of Microstructure and Mechanical Properties of Thermomechanically Processed Ultrahigh-Strength Steel. *Metallurgical and Materials Transactions A*. 2011;42(9):2742-2752.

9. Tian Y, Tang S, Wang BX, Wang ZD, Wang GD. Development and industrial application of ultra-fast cooling technology. *Science China Technological Sciences*. 2012;55(6):1566-1571.

10. Tang S, Liu Z, Wang G, Misra RDK. Microstructural evolution and mechanical properties of high strength microalloyed steels: Ultra Fast Cooling (UFC) versus Accelerated Cooling (ACC). *Materials Science and Engineering: A*. 2013;580:257-265.

11. Ravikumar SV, Jha JM, Mohapatra SS, Pal SK, Chakraborty S. Influence of Ultrafast Cooling on Microstructure and Mechanical Properties of Steel. *Steel Research International*. 2013;84(11):1157-1170.

12. Laasraoui A, Jonas JJ. Recrystallization of austenite after deformation at high temperatures and strain rates - Analysis and modeling. *Metallurgical Transactions A*. 1991;22(1):151-160.

13. National Standard of the People's Republic of China. *Petroleum and Natural Gas Industries-Steel Pipe for Pipeline Transportation Systems. GB/T 9711-2011*. Beijing: Chinese Standard Press; 2011. p. 27.

14. Girault E, Jacques P, Harlet P, Mols K, Van Humbeek J, Aernoudt E, et al. Metallographic Methods for Revealing the Multiphase Microstructure of TRIP-Assisted Steels. *Materials Characterization*. 1998;40(2):111-118.

15. Kim YW, Song SW, Seo SJ, Hong SG, Lee CS. Development of Ti and Mo micro-alloyed hot-rolled high strength sheet steel by controlling thermomechanical controlled processing schedule. *Materials Science and Engineering: A*. 2013;565:430-438.

16. Sung HK, Lee S, Shin SY. Effects of Start and Finish Cooling Temperatures on Microstructure and Mechanical Properties of Low-Carbon High-Strength and Low-Yield Ratio Bainitic Steels. *Metallurgical and Materials Transactions A*. 2014;45(4):2004-2013.

17. Zuo X, Zhou Z. Study of Pipeline Steels with Acicular Ferrite Microstructure and Ferrite-bainite Dual-phase Microstructure. *Materials Research*. 2015;18(1):36-41.

18. Lu J, Omotoso O, Wiskel JB, Ivey DG, Henein H. Strengthening Mechanisms and Their Relative Contributions to the Yield Strength of Microalloyed Steels. *Metallurgical and Materials Transactions A*. 2012;43(9):3043-3061.

19. Morales EV, Silva RA, Bott IS, Paciornik S. Strengthening mechanisms in a pipeline microalloyed steel with a complex microstructure. *Materials Science and Engineering: A*. 2013;585:253-260.

20. Pedrosa IRV, Castro RS, Yadava YP, Ferreira RAS. Study of phase transformations in API 5L X80 Steel in order to increase its fracture toughness. *Materials Research*. 2013;16(2):489-496.

21. Sung HK, Shin SY, Hwang B, Lee CG, Lee S. Effects of Cooling Conditions on Microstructure, Tensile Properties, and Charpy Impact Toughness of Low-Carbon High-Strength Bainitic Steels. *Metallurgical and Materials Transactions A*. 2013;44(1):294-302.

22. Park DB, Huh MY, Shim JH, Suh JY, Lee KH, Jung WS. Strengthening mechanism of hot rolled Ti and Nb microalloyed HSLA steels containing Mo and W with various coiling temperature. *Materials Science and Engineering: A*. 2013;560:528-534.

23. Gallego J, Rodrigues AR, Assis CLF, Montanari L. Second phase precipitation in ultrafine-grained ferrite steel. *Materials Research*. 2014;17(2):527-534.